

Evaluation of Zonal Detached Eddy Simulation $k - \omega$ and Scale Adaptive Simulation methods on a realistic rotor of a high-pressure compressor

C. Uribe^a, J. Marty^b, G. A. Gerolymos^c

a. ONERA, The French Aerospace Lab, 8 rue des Vertugadins, 92190 Meudon, France,
cedric.uribe@onera.fr

b. ONERA, The French Aerospace Lab, 8 rue des Vertugadins, 92190 Meudon, France,
julien.marty@onera.fr

c. Sorbonne Universités, UPMC univ Paris 06, CNRS, UMR 7190, Institut Jean Le Rond d'Alembert,
75005 Paris, France, georges.gerolymos@upmc.fr

Abstract :

Secondary flows prediction, like tip-leakage vortex flow or corner separation flow, are of primary importance in the correct evaluation of turbomachinery performances by CFD analysis. They cause additional losses and operating domain reduction. Since they exhibit strong fluctuating behaviors and separations, it is necessary to resolve a significant fraction of their turbulent content for accounting of their effects on the main flow. Hybrid RANS/LES methods and upgraded URANS approaches are interesting solutions to cope with this constraint with reasonable computational, treatment and storage costs. Among them, Zonal Detached Eddy Simulation (ZDES) method and Scale Adaptive Simulation (SAS) method have been respectively developed and improved in previous ONERA's studies. Particularly, ZDES method, originally based on the SA turbulence model, have been reformulated above the $k - \omega$ Menter model with SST correction in view to improve its behavior for predicting boundary layer separation due to progressive adverse pressure gradient. In this study, this new ZDES formulation (ZDES-SST) and the SAS method (SAS-SST) are assessed against ZDES-SA, URANS-SA and URANS-SST approaches on a realistic rotor flow of a high-pressure compressor with incoming stator wakes at one nominal operating point. URANS simulations are characterized by a low level of unsteadiness, matching RANS isospeed lines exploration. A clear discrepancy is present in URANS and RANS simulations depending of the turbulence model but ZDES-SA and ZDES-SST recover RANS-SST isospeed line which is closer to the experiment. Only ZDES approaches are able to capture fluctuations involved in tip flow, whereas SAS-SST results is more similar to URANS results than ZDES ones on this point but comes with higher stagnation pressure losses than URANS-SST.

Key words : Turbomachinery flow / unsteady flow / flow separation / tip-leakage flow / turbulence modeling / hybrid RANS/LES methods

1 Introduction

In order to improve turbomachinery performances it is necessary to correctly predict secondary and transitional flows inherent to this confined environment. Secondary flows can cause additional losses

and operating domain reduction. For example, tip-leakage vortex flow or corner separation flow on high pressure compressor blades lead to total pressure loss limiting turbomachinery efficiency and favoring emergence of hazardous axial instability (surge) or rotating stall.

Secondary flows exhibit strong fluctuating behaviors and separations which make their prediction quite challenging, often found inaccurate with current turbulence models used during design process. One reason lies in the error on turbulent fluctuation predictions when they are entirely modeled by statistical averaging (RANS - Reynolds Average Navier-Stokes). However, more accurate methods such as Large Eddy Simulations (LES) are difficult to use at high Reynolds number due to excessive computational, treatment and storage costs.

A trade-off can be found in hybrid RANS/LES methods such as ZDES (Zonal Detached Eddy Simulation) method developed at ONERA by Deck [2012]. ZDES method falls in the line with DES and DDES methods developed by Spalart et al. [1997] and Spalart et al. [2006] respectively. Through the main operating mode of ZDES method, boundary layers are treated by RANS modeling on their whole thickness to avoid near-wall excessive cost of LES method which is only used away of the walls. The interface between those two sub-methods is continuous. Its RANS sub-method is based on SA turbulence model [Spalart and Allmaras, 1992]. Following DES and DDES methods, its LES sub-method is obtained via a simple substitution of the characteristic length scale appearing in the destruction term of pseudo-viscosity transport equation of SA model by an hybrid length scale, hence decreasing eddy viscosity level to the order of a Smagorinsky [1963] subgrid scale model.

As demonstrated by Riéra [2014] the SA turbulence model used in the RANS sub-method of the current ZDES method makes difficult to predict turbomachinery flows at limit operating range because of its poor behavior near numerical surge line. A major reason is that RANS SA model tends to predict too massive or simply false flow separations, which is critical for such flows with corner flow separation [Marty et al., 2008]. A suggested remedy is to re-based the ZDES method on a more sophisticated RANS turbulence model as $k - \omega$ Menter [1994] turbulence model, which additionally can be easily combined with a laminar to turbulent transition model for future improvements of ZDES method.

Such ZDES method reformulation comes after numerous propositions for reformulating DES [Spalart et al., 1997] and DDES [Spalart et al., 2006] methods on $k - \omega$ turbulence models. At least three different substitution principles have been proposed: the first, from Travin et al. [2000], consisted to replace RANS characteristic length scale L_{RANS} by the hybrid length scale L_{DES} only in the destruction term (D_k) of turbulence kinetic energy transport equation. Numerous authors followed this idea, as Sainte-Rose et al. [2008], Mockett [2009] and Gritskevich et al. [2012], among others. The second, from Bush and Mani [2001], involved a substitution in D_k but also in the definition of turbulent viscosity ν_t , for an improved destruction of ν_t level from RANS region to LES region. The third, proposed by Reddy et al. [2014], is to apply this substitution only in the turbulent viscosity terms (ν_t) which appear in the mean field transport equations and the production term (P_k) of turbulence kinetic energy transport equation. As shown by Yin et al. [2015], this substitution principle facilitates the implementation of a dynamic procedure similar to that of Lilly [1966] in the subsequent DDES method based on Wilcox [1988] model. Deck [2012] suggested that ZDES method can also been reformulated above any RANS model following the idea of Travin et al. [2000]. This have been done by Arroyo-Callejo et al. [2016] above the $k - \omega$ Menter [1994] SST model in the ONERA's multiphysics computational platform CEDRE [Refloch et al., 2011], adapting ZDES method to unstructured grids framework.

Our study follows the reformulation of ZDES method within a structured grids frameworks inside the ONERA's *elsA* solver [Cambier et al., 2013]. Several ZDES $k - \omega$ Menter method formulations, related

to different substitution principles, have been assessed on three academic cases [Uribe et al., 2017] (a mixing layer flow, a backward facing step flow and a circular cylinder flow at $Re = 3900$). One of these formulations has been selected based on its capability (i) to allow the emergence and the correct development of Kelvin-Helmholtz instabilities and (ii) to ensure that boundary layers are treated by RANS modeling in their entire thickness.

Alternatively to hybrid RANS/LES methods, upgraded URANS approaches are interesting tools for resolving a variable fraction of the larger scales of turbulent motions, allowing a better representation of unsteady flows than URANS methods. Among them, the Scale Adaptive Simulation (SAS) approach of Menter and Egorov [2005, 2006, 2010] has been implemented in ONERA's *elsA* solver with an improvement from Benyoucef et al. [2012] dealing with the development of instabilities within mixing layers. This study focuses on the validation of the selected ZDES $k - \omega$ Menter formulation and the SAS approach on the same configuration as Riéra [2014] ZDES SA simulation i.e. a flow simulation of a realistic rotor of a high-pressure compressor with incoming stator wakes. For the sake of completeness, URANS SST approach have also been tested. Simulations are carried out on the same mesh and numerical framework as W. Riéra ones for appropriate comparison with their ZDES SA and URANS SA results, and with experimental data.

2 Evaluated methods

In this study, URANS, SAS (Scale Adaptive Simulation [Menter and Egorov, 2005]) and ZDES (Zonal Detached Eddy Simulation [Deck, 2012]) methods are performed on a very fine mesh which satisfies the ZDES mesh requirements in term of $\Delta x^+ (< 200)$, $\Delta y^+ (< 1)$ and $\Delta z^+ (< 200)$ where x , y and z are the streamwise, normalwise and crosswise directions, respectively. With these methods, the nominal operating point is only simulated. Nonetheless, RANS simulations are performed on a coarser mesh (fine mesh for RANS simulations) in order to highlight the nominal operating point with respect to the nominal isospeed. SAS and ZDES methods are detailed in this section

2.1 Zonal Detached Eddy Simulation methods

Original formulation

The original Zonal Detached Eddy Simulation (ZDES) method [Deck, 2012] is based on the one-equation Spalart and Allmaras [1992] (SA) RANS model whose pseudoviscosity $\tilde{\nu}$ transport equation is partially recalled here:

$$\frac{\partial \rho \tilde{\nu}}{\partial t} + \text{div}(\rho \tilde{\nu} \underline{U}) = P_{\tilde{\nu}} - D_{\tilde{\nu}} + \frac{1}{\sigma} \left[\text{div} \left((\mu + \rho \tilde{\nu}) \underline{\text{grad}}(\tilde{\nu}) \right) + c_{b2} \rho \underline{\text{grad}}(\tilde{\nu}) \cdot \underline{\text{grad}}(\tilde{\nu}) \right] \quad (1)$$

$$P_{\tilde{\nu}} = c_{b1} \tilde{S} \rho \tilde{\nu}, \quad D_{\tilde{\nu}} = \rho c_{w1} f_w \left(\frac{\tilde{\nu}}{d_w} \right)^2, \quad \mu_t = f_{v1} \rho \tilde{\nu} \quad (2)$$

with $P_{\tilde{\nu}}$ the production term, $D_{\tilde{\nu}}$ the destruction term, \tilde{S} the modified vorticity magnitude, f_w and f_{v1} some of the model near-wall damping functions and σ , c_{b1} , c_{b2} , c_{w1} some of the model constants.

Following a formulation principle inherited from DES97 [Spalart et al., 1997] and DDES [Spalart et al., 2006] methods, the ZDES one is built by replacing the characteristic length scale L_{RANS} of the turbulence RANS model by an hybrid length scale L_{DES} dependent of local subgrid length scale Δ and local properties of the flow. The objective is to enhance the importance of destruction term for producing a level of turbulent viscosity comparable to an LES sub-grid Smagorinsky model [Smagorinsky, 1963],

and hence disposing of an URANS method which can act as an LES method in pertinent locations, supposing the adequate numerical framework. In the ZDES method based on SA model (ZDES-SA), the RANS length scale L_{RANS} is identified as the wall distance d_w which appears in the destruction term and near-wall corrections (f_w , \tilde{S}). Hence $D_{\tilde{\nu}} = \rho c_{w1} f_w (\tilde{\nu}/d_w)^2$ becomes $D_{\tilde{\nu}} = \rho c_{w1} f_w (\tilde{\nu}/L_{DES})^2$, $f_w(L_{RANS})$ becomes $f_w(L_{DES})$ and $\tilde{S}(L_{RANS})$ becomes $\tilde{S}(L_{DES})$. The definition of L_{DES} depends of the ZDES mode selected L_{DES} : L_{RANS} (for mode 0), L_{DES}^I (for mode 1), L_{DES}^{II} (for mode 2) and L_{DES}^{III} (for mode 3). As reminded by Fig. 1, these ZDES modes are adapted to different flow problems and

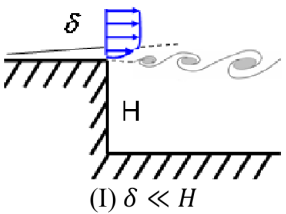
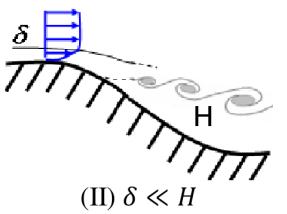
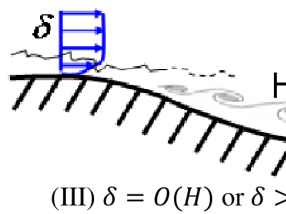
Zonal Detached Eddy Simulation (ZDES)			
	Mode 1	Mode 2	Mode 3
Flow category			
Applications	Base flow, free shear flows, spoilers, steps, slat/flap cove, etc.	Buffet, flaps, duct flows, nacelle intake, etc.	Corner flows, turbulent boundary layers, separation onset on high-lift devices, shallow separations, etc.

Figure 1: Classification of typical flow problems. I: separation fixed by the geometry, II: separation induced by a pressure gradient on a curved surface, III: separation strongly influenced by the dynamics of the incoming boundary layer (adapted from Deck [2012], Deck et al. [2014]).

each one can be used in the same simulation on different regions of the computational domain. This spatial specialization possibility, with associated grid requirements range, is one of the ZDES advantage compared to DDES method. Despite the following description of the method, more details are given in Deck [2012]. The mode 0 correspond to pure RANS (or URANS) and allows the user to design a mesh whose some parts can be as light as pure RANS mesh. The mode 1 is adapted to configurations where the separation is fixed by the geometry (*a priori* known separation position) since its formulation is related to DES97 ones:

$$\text{ZDES SA Mode 1 : } \begin{cases} L_{DES}^I = \min(L_{RANS}, L_{LES}) \\ L_{RANS} = d_w, \quad L_{LES} = C_{DES} \Delta_{DES}^I, \quad C_{DES} = 0.65 \\ \Delta_{DES}^I = \Delta_{vol} \text{ or } \Delta_{\omega} \text{ (user's choice)} \\ \text{if } L_{DES}^I = L_{LES} \text{ then } f_{v1} = 1, f_{v2} = 0 \text{ and } f_w = 1 \end{cases} \quad (3)$$

Like DES97 method, C_{DES} value comes from Shur et al. [1999] calibration against decaying homogeneous isotropic turbulence experiment of Comte-Bellot and Corrsin [1971]. Instead of relying on the maximum length of the cell for the calculation of the subgrid length scale ($\Delta_{max} = \max(\Delta_x, \Delta_y, \Delta_z)$), the ZDES mode 1 allow user to choose between a subgrid length scale based on the cell volume Δ_{vol} or a subgrid length scale based on the vorticity normal cell section Δ_{ω} , well suited to ensure a rapid switch into the LES mode for anisotropic grid [Chauvet et al., 2007, Deck, 2012]. Since the RANS/LES interface position is directly dependent of mesh grid via Δ_{DES}^I , ZDES mode 1, as DES97, is inappropriate for protecting boundary layers of an LES treatment. On the other hand, with an adapted mesh in order to avoid Model Stress Depletion and Grid Induced Separation, mode 1 is a practical way to force a rapid switch into LES treatment after a geometry singularity known for triggering massive flow separation, like an airfoil trailing edge, a projectile base or a backward facing step.

The mode 2, following DDES method, use the algebraic function f_d for ensuring a RANS treatment of boundary layers in their entire thickness. Hence it is adapted to configurations where massive separations occur but their positions are *a priori* unknown, like for adverse pressure gradient induced separation. Massive qualification means a separation significantly bigger than the upstream boundary layer thickness. An important beneficial difference from DDES method relies in the fact that Δ_{DDES}^{II} leaves the Δ_{max} value for the Δ_{vol} (or Δ_ω following user's choice) one from the limit of boundary layers ($f_d > 0.8$) to far-field. This ensures a shorter delay in the formation of instabilities away from the walls.

$$\text{ZDES SA Mode 2 : } \begin{cases} L_{DDES}^{II} = L_{RANS} - f_d \times \max(0, L_{RANS} - L_{LES}) \\ L_{RANS} = d_w, \quad L_{LES} = C_{DES} \Delta_{DDES}^{II}, \quad C_{DES} = 0.65 \\ \Delta_{DDES}^{II} = \begin{cases} \Delta_{max} & \text{if } f_d \leq f_{d0} \\ \Delta_{vol} \text{ or } \Delta_\omega \text{ (user's choice)} & \text{if } f_d > f_{d0} \end{cases}, \quad f_{d0} = 0.8 \end{cases} \quad (4)$$

$$f_d = 1 - \tanh \left[(C_{d1} r_d)^{C_{d2}} \right], \quad r_d = \frac{\nu + \nu_t}{\sqrt{U_{i,j} U_{i,j}} K^2 d_w^2}, \quad C_{d1} = 8, \quad C_{d2} = 3 \quad (5)$$

The mode 3 is related to a wall-modeled LES method, where boundary layers are resolved by LES treatment from a user defined RANS/LES interface to far-field. This is an appropriate solution for separation which are determined by the internal dynamics of incoming boundary layer [Deck and Laraufie, 2013]. As this mode is not used in the present study, we refer to the original paper [Deck, 2012] and to the works of Laraufie et al. [2011] and Renard and Deck [2015] for a full description of mode 3.

Formulation of ZDES $k - \omega$ method

The Zonal Detached Eddy Simulation method developed and used in this study, the ZDES $k - \omega$, differs from the original one, the ZDES SA, by its underlying turbulence RANS model. It is based on the $k - \omega$ model of Menter [1994] with Shear-Stress Transport (SST) correction. This two equations RANS turbulence model is recalled hereafter.

$$\frac{\partial \rho k}{\partial t} + \text{div}(\rho k \underline{U}) = P_k - D_k + \text{div} \left[(\mu + \sigma_k \mu_t) \underline{\text{grad}}(k) \right] \quad (6)$$

$$\frac{\partial \rho \omega}{\partial t} + \text{div}(\rho \omega \underline{U}) = P_\omega - D_\omega + \text{div} \left[(\mu + \sigma_\omega \mu_t) \underline{\text{grad}}(\omega) \right] + (1 - F_1) CD_{k\omega} \quad (7)$$

$$P_k = \left[-\frac{2}{3} (\rho k + \mu_t \text{div}(\underline{U})) \underline{I} + 2\mu_t \underline{S} \right] : \underline{\underline{\text{grad}}}(\underline{U}), \quad D_k = \beta^* \rho k \omega \quad (8)$$

$$P_\omega = \frac{\gamma \rho}{\mu_t} P_k, \quad D_\omega = \beta \rho \omega^2, \quad CD_{k\omega} = 2 \frac{\rho \sigma_\omega^2}{\omega} \underline{\underline{\text{grad}}}(k) \cdot \underline{\underline{\text{grad}}}(\omega) \quad (9)$$

$$\mu_t = \frac{\rho k}{\omega_{SST}}, \quad \omega_{SST} = \max \left(\omega; \frac{1}{a_1} F_2 \times \sqrt{2 (\underline{S} : \underline{S})} \right), \quad a_1 = 0.31 \quad (10)$$

with $\beta^* = 0.09$ and the von Kármán constant $K = 0.41$. Each other model constants ϕ are calculated as $\phi = F_1 \phi_1 + (1 - F_1) \phi_2$ with the following ϕ_1 and ϕ_2 set:

$$\begin{aligned}\sigma_{k1} &= 0.85, & \beta_1 &= 0.075, & \sigma_{\omega1} &= 0.5, & \gamma_1 &= \frac{\beta_1}{\beta^*} - \sigma_{\omega1} \frac{K^2}{\sqrt{\beta^*}} \\ \sigma_{k2} &= 1.0, & \beta_2 &= 0.0828, & \sigma_{\omega2} &= 0.856, & \gamma_2 &= \frac{\beta_2}{\beta^*} - \sigma_{\omega2} \frac{K^2}{\sqrt{\beta^*}}\end{aligned}\quad (11)$$

$$F_1 = \tanh(\zeta^4), \quad \zeta = \min \left[\max \left(\frac{\sqrt{k}}{0,09\omega d_w}; \frac{500\nu}{\omega d_w^2} \right); \frac{4\rho\sigma_{\omega2}k}{CD_{k\omega} d_w^2} \right] \quad (12)$$

$$F_2 = \tanh(\chi^2), \quad \chi = \max \left(2 \frac{\sqrt{k}}{0,09\omega d_w}; \frac{500\mu}{\rho\omega d_w^2} \right) \quad (13)$$

Such ZDES method reformulation comes after numerous propositions for reformulating DES [Spalart et al., 1997] and DDES [Spalart et al., 2006] methods on $k - \omega$ turbulence models.

Travin et al. [2000] proposed a generalization of DES method applicable to any RANS model, presented above $k - \omega$ Menter [1994] model and based on the sole length scale substitution in the destruction term (D_k) of turbulence kinetic energy transport equation. This length scale substitution implies to identify the RANS characteristic length scale as $L_{RANS} = \sqrt{k}/\beta^*\omega$ and to replace it by the chosen hybrid length scale L_{DES} . Hence $D_k = \beta^*\rho k\omega = \rho k^{3/2}/L_{RANS}$ becomes $D_k = \rho k^{3/2}/L_{DES}$. Numerous DES or DDES methods [Menter and Kuntz, 2002, Travin et al., 2006, Bunge et al., 2007, Sainte-Rose et al., 2008, Mockett, 2009, El Akoury et al., 2009, Guilmineau et al., 2011, Zhou et al., 2017] used this principle on various $k - \omega$ models. Gritskevich et al. [2012, 2013] optimized f_d shielding function coefficients for the subsequent DDES method based on $k - \omega$ Menter [1994] model with SST correction.

Bush and Mani [2001] applied the same length scale substitution in D_k but also in the definition of turbulent viscosity, hence $\nu_t = k/\omega$ is rewritten as $\nu_t = \beta^* L_{RANS} \sqrt{k}$ and becomes $\nu_t = \beta^* L_{DES} \sqrt{k}$. Kok et al. [2004] follow this idea for building their X-LES method above the TNT $k - \omega$ model [Kok, 2000]. Yan et al. [2005, 2007] and Michel et al. [2007] evaluated the same double length scale substitution on $k - \omega$ Wilcox [1988] model, demonstrating its better behavior compared to the unique D_k substitution for decreasing ν_t level from RANS region to LES region. It is also the departure point of Chuangxin et al. [2017] for building their dynamic delayed detached-eddy above $k - \omega$ Menter [1994] model with SST correction.

Reddy et al. [2014] proposed another substitution principle by which the length scale substitution is applied only in the turbulent viscosity terms (ν_t) which appear in the mean field transport equations and the production term (P_k) of turbulence kinetic energy transport equation. Those terms are reformulated as $\nu_t = \omega(L_{RANS})^2$ and becomes $\nu_t = \omega(L_{DES})^2$. As showed by Yin et al. [2015], this substitution principle facilitates the implementation of a dynamic procedure similar to that of Lilly [1966] in the subsequent DDES method based on Wilcox [1988] model.

In the scope of this study, ZDES $k - \omega$ is built identifying the characteristic length scale $L_{RANS} = \sqrt{k}/\beta^*\omega$, often taken as the integral scale of turbulence, and replacing it by the hybrid length scale L_{DES} . This is done only in the destruction term of turbulent kinetic energy, D_k , as originally accomplished by Travin et al. [2000] for DES97 method or suggested and applied for ZDES method by Deck [2012] and Arroyo-Callejo et al. [2016] - in the unstructured grids framework of multiphysics computational platform CEDRE [Refloch et al., 2011] - respectively. Hence $D_k = \beta^*\rho k\omega = \rho k^{3/2}/L_{RANS}$ becomes $D_k = \rho k^{3/2}/L_{DES}$. The mode 1 differs only of its ZDES SA counterpart by the definition of C_{DES} taken as the Travin et al. [2000] ones: $C_{DES} = (1 - F_1) C_{DES}^{k-\varepsilon} + F_1 C_{DES}^{k-\omega}$, with $C_{DES}^{k-\varepsilon} = 0.61$ and $C_{DES}^{k-\omega} = 0.78$. Mode 2 differs also by the protection function f_f of Fan et al. [2004] which have been successfully used by Sainte-Rose et al. [2008] and Arroyo-Callejo et al. [2016]. This protection

function is applied in the definition of L_{DES}^{II} : $L_{DES}^{II} = L_{RANS} - f_f \times \max(0, L_{RANS} - L_{LES})$ and is defined by $f_f = 1 - \tanh(\psi^4)$ with $\psi = \max\left(\frac{\sqrt{k}}{0.09\omega d_w}; \frac{500\mu}{\rho\omega d_w^2}\right)$. Either with mode 1 or mode 2, SST correction is limited to RANS regions since this has no physical justification in LES methods. This is done as smoothly as the RANS/LES transition occurs thanks to a general RANS/LES sensor evaluation: $\mu_t = \rho k / \omega_{ZDES-SST}$ with $\omega_{ZDES-SST} = \lambda \times \omega_{SST} + (1 - \lambda) \times \omega$ and $\lambda = 1 - \frac{L_{DES} - L_{LES}}{L_{RANS} - L_{LES}}$. Hence, λ varies from 0 in pure RANS regions, as f_d and f_f inside boundary layers, to 1 in pure LES regions, as f_d and f_f outside boundary layers. Application of Zheng limiter [Zheng et al., 1998] is treated as SST correction.

Nevertheless, an important behavior divergence between ZDES SA and ZDES $k - \omega$ must be raised: L_{RANS} evolution is not anymore monotonically growing with wall distance but evolves freely following flows physics. Hence a situation where $L_{RANS} < L_{LES}$ can occur away from walls, as experienced by Sainte-Rose et al. [2009], resulting in a RANS treatment region where ZDES is expected to work in LES mode. Apart from a grid refinement, a remedy can be found in the following alternative formulation qualified as ZDES $k - \omega$ *h.v.* with *h.v.* for hardened version. The idea is to proceed as ZDES SA i.e. by comparing d_w and L_{LES} for deciding either if L_{RANS} or L_{LES} will be used as L_{DES} .

$$\text{ZDES } k - \omega \text{ h.v.: } \begin{cases} L_{DES}^I = \begin{cases} L_{RANS} & \text{if } d_w \leq L_{LES} \\ L_{LES} & \text{if } d_w > L_{LES} \end{cases} \\ L_{DES}^{II} = \begin{cases} L_{RANS} & \text{if } d_w \leq L_{LES} \\ (1 - f_f) L_{RANS} + f_f L_{LES} & \text{if } d_w > L_{LES} \end{cases} \end{cases} \quad (14)$$

This alternative formulation has not been used in the scope of this study.

2.2 Scale Adaptive Simulation method

Original formulation

The Scale Adaptive Simulation (SAS) method of Menter and Egorov [2005, 2006, 2010] can be considered of an improved URANS model which mimics the behavior of hybrid RANS/LES methods: when the flow is attached, the standard RANS solution is obtained; when the flow is separated, an extra term in the scale equation becomes active and reduces the eddy viscosity, which allows capturing large turbulent eddies and resolve part of the turbulence spectrum. The original SAS method relies on the $k - \omega$ model of Menter [1994] with Shear-Stress Transport (SST) correction as presented in eq. (6) to (13). It differs from RANS since the extra term, Q_{SAS} , is added to $\rho\omega$ transport equation (7) resulting in (15).

$$\frac{\partial \rho\omega}{\partial t} + \text{div}(\rho\omega \underline{U}) = P_\omega - D_\omega + \text{div}\left[(\mu + \sigma_\omega \mu_t) \underline{\text{grad}}(\omega)\right] + (1 - F_1) CD_{k\omega} + Q_{SAS} \quad (15)$$

The Q_{SAS} term, which is responsible for the decrease of eddy viscosity in case of flow instabilities, has the following expression:

$$Q_{SAS} = \max\left[\rho \zeta_2 K S^2 \left(\frac{L}{L_{vK}}\right)^2 - C \frac{2\rho k}{\sigma_\Phi} \max\left(\frac{1}{k^2} \underline{\text{grad}}(k) \cdot \underline{\text{grad}}(k), \frac{1}{\omega^2} \underline{\text{grad}}(\omega) \cdot \underline{\text{grad}}(\omega)\right), 0\right] \quad (16)$$

where the magnitude of the strain rate tensor S and related constants are defined as:

$$S = \sqrt{2(\underline{S} : \underline{S})}, \quad \zeta_2 = 3.51, \quad \sigma_\Phi = \frac{2}{3}, \quad C = 2 \quad (17)$$

In the Q_{SAS} expression, L is the length scale deduced from the turbulent scales transported by the model: $L = k^{\frac{3}{2}}/\varepsilon = \sqrt{k}/C_{\mu}^{\frac{1}{4}}\omega$ and L_{vK} is a 3D generalization of the von Kármán length scale expression coming from the boundary layer theory and expressed by (using $\|\Delta\mathbf{U}\|$, the norm of the Laplacian of the velocity vector):

$$L_{vK} = K \frac{S}{\|\Delta\mathbf{U}\|}, \quad \|\Delta\mathbf{U}\| = \sqrt{\frac{\partial^2 U_i}{\partial x_j^2} \frac{\partial^2 U_i}{\partial x_j^2}} \quad (18)$$

αL correction

It can be shown that in the original SAS expression of Menter, the von Kármán length scale goes to infinity in the center of a 2D mixing layer. This implies that the Q_{SAS} term is zero in a region close to the mixing layer center. This unwanted feature prevents or causes delay to the development of mixing layer instabilities (Kelvin-Helmholtz instabilities). A correction was introduced by Benyoucef et al. [2012] to limit the upper bound of the von Kármán length scale:

$$\widetilde{L}_{vK} = \min(L_{vK}, F_1 L_{vK} + [1 - F_1] \alpha L) \quad (19)$$

where α is a constant (default value equal to 2.5). The blending function F_1 (see Eq. (12)) is present here to prevent this new expression to be active in the inner boundary layer and ensure a RANS behavior in the attached boundary layer.

3 Experimental facility

In the present study, the computational domain of all simulations is the first rotor of the research compressor CREATE whose characteristics are summarized in table 1. The experimental compressor is located at the LMFA laboratory (Lyon, France) [Ottavy et al., 2012, Touyeras and Villain, 2004]. This is an axial flow compressor which comprises $3^{1/2}$ stages as shown in figure 2 and in table 2 which details the blade number of each row. This research compressor is representative of the median and rear stages of modern high pressure compressors. As there is a spatial periodicity of $2\pi/16$, measurements are carried out over a sector of 22.5° and should contain all the spatial information for stabilized operating points at least and are very useful for rotor-stator interaction analysis. In the present study, as only the first rotor is simulated (at design operating point), measurements are carried out with both pneumatic and unsteady pressure probes, detailed by Mersinligil et al. [2012], which are located in the axial sections 25A and 26A, visible in figure 2. Moreover, LDA measurements are available in different axial sections along with the first rotor chord.

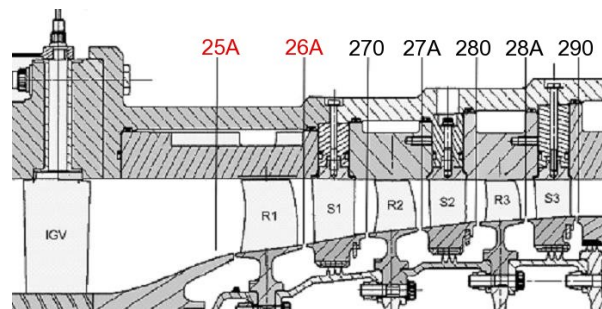


Figure 2: CREATE compressor meridian view.

Table 1: Characteristics at design operating point

Outer casing diameter	0.52 m
Rotating speed	11543 rpm
Mass flow	12.7 kg.s ⁻¹
Inlet Mach number at tip of R1	0.92

Table 2: Blade number for the rows

Row	IGV	R1	S1	R2	S2	R3	S3
Blade number	32	64	96	80	112	80	128

4 Numerical framework

4.1 Computational domain, grid description and boundary conditions

As previously mentioned, only the first rotor is simulated. The zonal approach affects the mesh refinement as follows: a RANS type mesh upstream of the blade, and DES type mesh from the leading edge onward, i.e. a LES resolution mesh except on the wall. The normalized wall cell dimension normal to the wall fulfils Δy^+ of the order of 1 in every zone. However, its wall parallel counterparts differ depending on the zones: upstream of R1, Δx^+ (streamwise direction) is between 400 and 500 and Δz^+ (spanwise direction) less than 100; in the vicinity of the blades, Δx^+ and Δz^+ are respectively of the order of 200-300 and 100; and downstream of the blades, the mesh is progressively coarsened to 1700 for Δx^+ and 150 for Δz^+ so as to avoid numerical reflections. The computational domain is shown in figure 3. The whole grid comprises $N_{xyz} = 88$ million points in order to model 1/32 of the compressor, i.e. two channels of R1, which corresponds to the inlet guide vane blade count (table 2). A coarser mesh i.e. a fine mesh adapted to RANS method but too coarse for ZDES (6 million points for one rotor passage), is used to compute the nominal isospeed with RANS methods and the following numerical methods. These simulations are used as references.

Despite only the first rotor is simulated, the wakes and vortices coming from the IGV are taken into account in all simulations by using specific inlet conditions. The inlet boundary of the computational domain is set to section 25A of the experimental test rig, located between the IGV and the R1, in order to set experimental values at the inlet boundary. The specific boundary condition at the inlet consists in a rotating distortion cartography (2D map comprises the IGV wakes and vortices), whose method was used for centrifugal compressor by Tartousi et al. [2011], based on a Fourier decomposition with 60 harmonics of the two dimensional map of the flow.

The outlet boundary of the computational domain is defined at two axial chords downstream the R1. At this boundary, the back pressure is prescribed using a radial equilibrium law and has been adapted to match the probe measurements at the tip in terms of axial momentum. It should be noticed that the first stator S1 effects (e.g. potential effects) are not taken into account in the present investigation. All walls are considered as adiabatic and a no-slip condition is used. Finally, a classic rotation periodicity condition is set at the azimuthal boundaries.

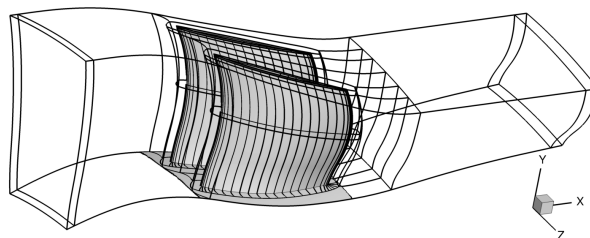


Figure 3: Computational domain for the calculations on the first rotor of CREATE.

4.2 Numerical methods

The CFD solver used in this study is the ONERA's software *elsA* [Cambier et al., 2013]. This solver is based on a cell centered finite volume approach to solve the Navier-Stokes equations on a structured multi-block grid. The spatial discretization scheme [Mary et al., 2000] for the inviscid fluxes is based on the third order accurate Advection Upstream Splitting Method for low Mach numbers (AUSM+P), initially developed by Edwards and Liou [1997]. A classic second order centred formulation is used for the viscous fluxes.

The time integration is based on the second order accurate Gear scheme. The time step is set to $1.6 \cdot 10^{-7}$ s which leads to a Courant-Friedrich-Lewy number lower than 1 except for the boundary layers. It corresponds to 1000 time steps per IGV passing period. The use of 8 sub-iterations per time-step is required to reach a decay superior to one order of magnitude for the residuals. This criteria is a compromise between precision and cost of the computation and takes into account the small time step involved [Daude, 2007].

More details concerning this numerical test bench are given in Riéra et al. [2016], especially the zonal configuration for ZDES approach. Nonetheless, it should be noticed that all URANS, SAS and ZDES simulations are performed on the same mesh, with the same boundary conditions and the same numerical methods.

In the following chapters, for homogenization notation reasons, ZDES $k-\omega$ method will be referred as ZDES-SST whereas SAS approach with αL correction will be referred as SAS-SST.

5 Results and discussion

5.1 Time-averaged field analysis

In the present investigation, the main validation is based on compressor performances and radial profiles upstream and downstream of the first rotor. After the transient part of the simulation, computational data are time-averaged over $20T$ where T is the passage-time period of the IGV with respect to the first rotor. Then they are azimuthally-averaged to obtain radial profiles. These data are finally averaged spanwise in order to compute the rotor performances. It should be noted that due to time constraint, time-averaged ZDES-SST results were averaged only on $3T$, hence there are not fully statistically converged.

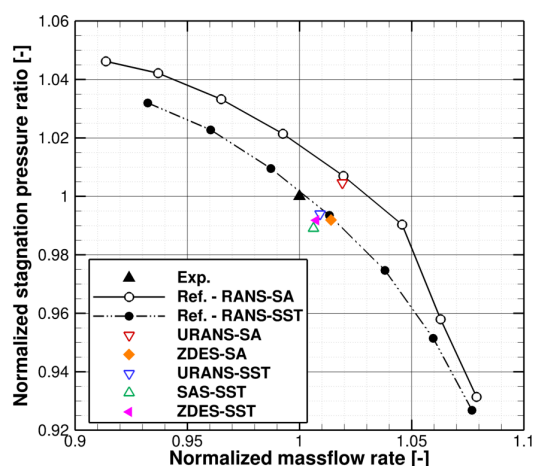


Figure 4: Performances of the first rotor: stagnation pressure ratio vs. massflow

Figure 4 depicts the normalized stagnation pressure ratio evolution along with the normalized massflow. In stable branch of the isospeed line, the stagnation pressure ratio increases with the massflow. Two references (RANS-SA and RANS-SST) are used to highlight the trend of the nominal isospeed which depends on the RANS turbulence model. As previously mentioned, these simulations are performed on a mesh which is too coarse for ZDES but is

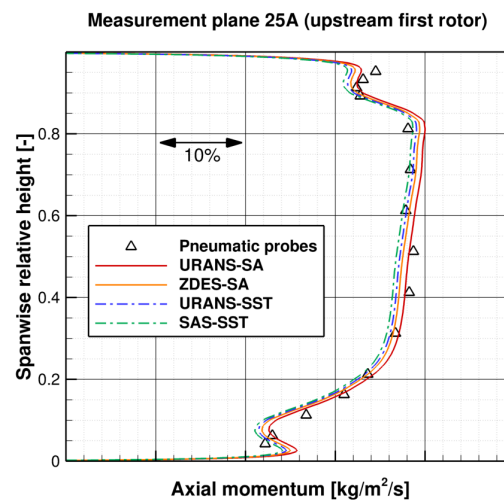


Figure 5: Axial momentum profile at the inlet (experimental plane)

fine for RANS method. At the nominal point, RANS-SA overestimates the stagnation pressure ratio by 0.8% and the massflow by 2% while RANS-SST is very close to experimental value.

URANS-SA, URANS-SST, SAS-SST, ZDES-SA and ZDES-SST simulations are performed on the finest mesh well adapted to ZDES method. The comparison between URANS-SA and ZDES-SA is detailed in Riéra et al. [2016]. As unsteadinesses are quite small in URANS computations, it should be noticed that the mesh convergence is obtained as performances are very similar between RANS-SA and URANS-SA on one hand and between RANS-SST and URANS-SST on the other hand. Thus this mesh insensitivity concerns as SA turbulence model as SST one. SAS approach underestimates the stagnation pressure rise by 1.1% and overestimates the massflow by 0.6%. As the stagnation pressure increases with massflow in the stable part of the isospeed, this means that the isospeed with SAS is quite different from URANS one and the stagnation pressure losses are probably higher in SAS computation.

The overall performances predicted by ZDES-SST are quite close to those of ZDES-SA and SAS-SST. The massflow is overestimated by less than 1% while the stagnation pressure ratio is underestimated by less than 1%. The stagnation pressure ratio is similar for both ZDES computations. Nonetheless, as the massflow is slightly smaller, the blockage is a little bit higher for ZDES-SST. The overall performances of ZDES-SST are located between those of SAS-SST and URANS-SST.

Figure 5 shows the radial distribution of the axial momentum at the inlet of the computational domain which is also the experimental plane upstream of the first rotor. All numerical results are close to experimental data. The trend of radial profile is well captured by all methods. Nonetheless, the gradient at casing is underestimated by all simulations. The small discrepancy at the hub is due to the absence of a leakage flow resulting from the gap between rotating and fixed hub (figure 2). The discrepancies between numerical results is directly linked to the difference of massflow between them (figure 4). Figure 6 depicts the radial distribution of absolute stagnation pressure and absolute deviation angle in the experimental plane 26A located downstream of the first rotor. Two kinds of experimental data are available for stagnation pressure: pneumatic probe and unsteady pressure probe. The measurements of the last one are time-averaged and plotted here. In figure 6(a), as shown by Riéra et al. [2016], ZDES-SA improves significantly the radial profile of absolute stagnation pressure by comparison to URANS-SA. Similar improvement is obtained using the SST turbulence model instead of the SA one. Close to the casing, only ZDES-SA and SAS-SST are able to well capture the absolute stagnation pressure gradient. At 82.5% spanwise, the comparison between numerical results and experimental data shows that only ZDES-SA is able to well capture the tip leakage vortex location. With URANS methods, the vortex is predicted at higher spanwise location while with SAS-SST the tip leakage vortex is more radially convected (absolute stagnation pressure peak is located around 79% spanwise). At the hub, as the recirculation induced by the gap between rotating and fixed hub is not taken

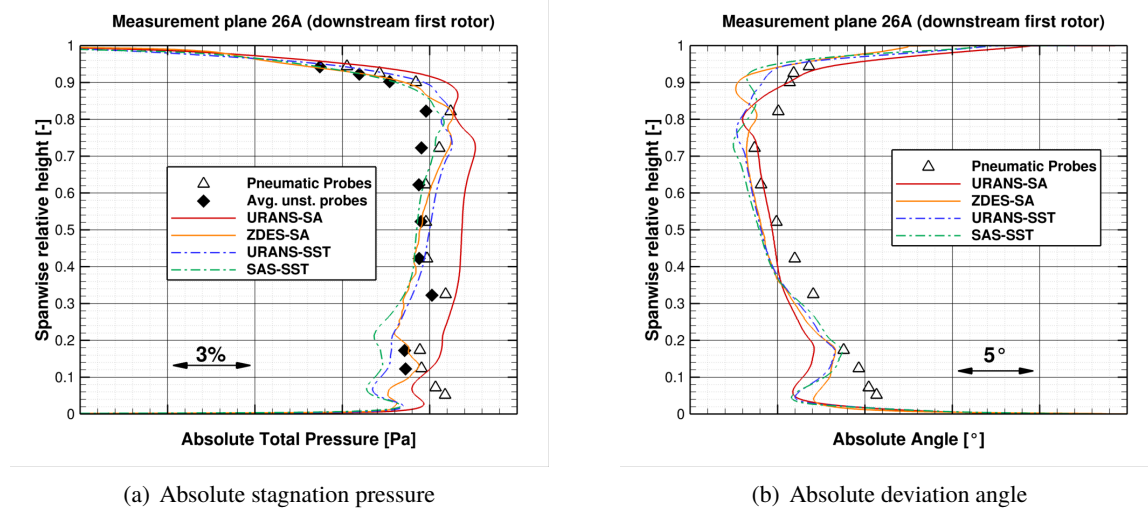


Figure 6: Absolute stagnation pressure and absolute deviation angle at the experimental plane downstream the first rotor (plane 26A).

into account in all simulations [Marty and Aupoix, 2012], the absolute stagnation pressure is underestimated. Moreover, URANS-SST and SAS-SST predicts a slightly wider separation over the suction side of the blade, close to the hub junction which amplifies the underestimation of stagnation pressure. With URANS-SST and SAS-SST, stagnation pressure losses are higher than ZDES-SA and URANS-SA. In figure 6(b), the deviation angle is mainly underestimated, especially in region of secondary flows: leakage flow at the hub and tip leakage flow around 80% spanwise. Nonetheless, only ZDES and SAS methods highlight the tip leakage vortex at this plane (slightly increase of absolute deviation angle between 80 and 85% spanwise). The experimental point number is not sufficient to prove which methods is better than the other ones. It should be noticed that, at the hub, the underestimation due to the absence of leakage flow is increased by the prediction of small separation over the blade, especially for URANS-SST and SAS-SST as shown by the angle gradient around 10% spanwise. As the acquired signal is too small to perform a time-average similar to other simulations, the radial distributions of ZDES-SST are not plotted. The simulation duration is the main limitation and prevent to show the real behavior of ZDES-SST.

Figure 7 depicts the time-averaged entropy variation of all simulations at three sections at 22, 31, and 46% of the axial chord, respectively. As all walls are considered as adiabatic, the entropy field is directly linked to stagnation pressure loss [Denton, 1993]. Both URANS computations predict a large area of high losses linked to the dissipated tip leakage vortex. This tip leakage vortex can be still observed on both ZDES results and losses are smaller than URANS ones. The SAS-SST computation predicts smaller losses than URANS-SST and the impact of Q_{SAS} is clearly visible as the tip leakage vortex is less dissipated. Nonetheless, the tip leakage vortex predicted by SAS-SST is still closer to URANS-SST than ZDES-SST numerical results.

5.2 Tip flow analysis

Figure 8 depicts the isosurface of Q criterion coloured by the normalized helicity (cf. Riéra et al. [2016] for the definition) and the entropy variation field at the section 31% X/C for the five unsteady simulations (URANS-SST, SAS-SST, ZDES-SST, URANS-SA and ZDES-SA). URANS results are rather similar as only the tip leakage vortex and the induced vortex are captured up to the plane 31% X/C and their locations are quite the same. At this plane, the weak shock disrupts the vortices which are subsequently dissipated. It should be noticed that the induced vortex is still visible after this axial plane with URANS-SST. With SAS-SST method, the tip leakage vortex is observed on a slightly longer distance. However the dissipation occurs quickly and the vortex is not visible after 46% X/C. The main discrepancy between URANS-SST and SAS-SST is the prediction of a secondary leakage vortex by SAS-SST. This vortex can be seen as a very large eddy. By comparison to SAS-SST, ZDES-SST and ZDES-SA exhibit multiple flow patterns and numerous secondary tip-leakage vortices. The turbulence spectrum

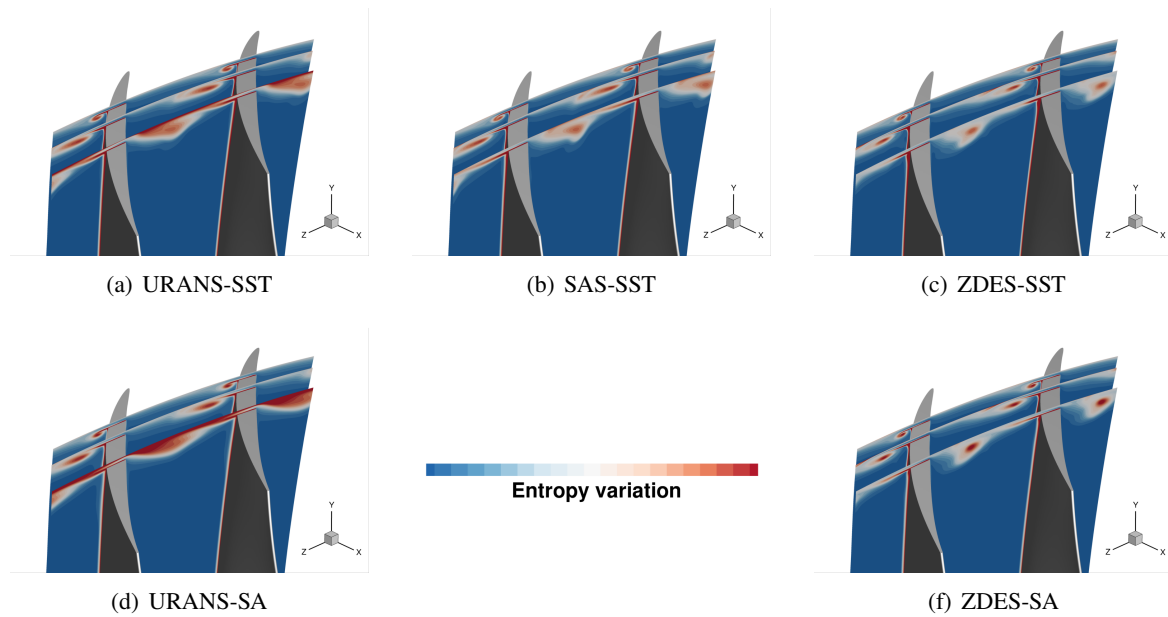


Figure 7: Time averaged entropy variation field in three axial planes along the chord.

is more rich as the coherent structures have very different length scales. This is the main benefit to use ZDES approaches. The patterns are quite similar between both ZDES simulations. Only the ZDES methods are able to capture the interaction between the tip flows of two adjacent blades. As shown by Riéra et al. [2016], the tip leakage vortex disrupts before the tip flow impinges the pressure side of the adjacent blade, generating both a double tip leakage flow (a tip leakage flow takes a part of the generation of another tip leakage flow) and numerous small eddies in the vicinity of the trailing edge of the adjacent blade.

The instantaneous entropy variation field is depicted in figure 9 at four axial position (one column per axial posi-

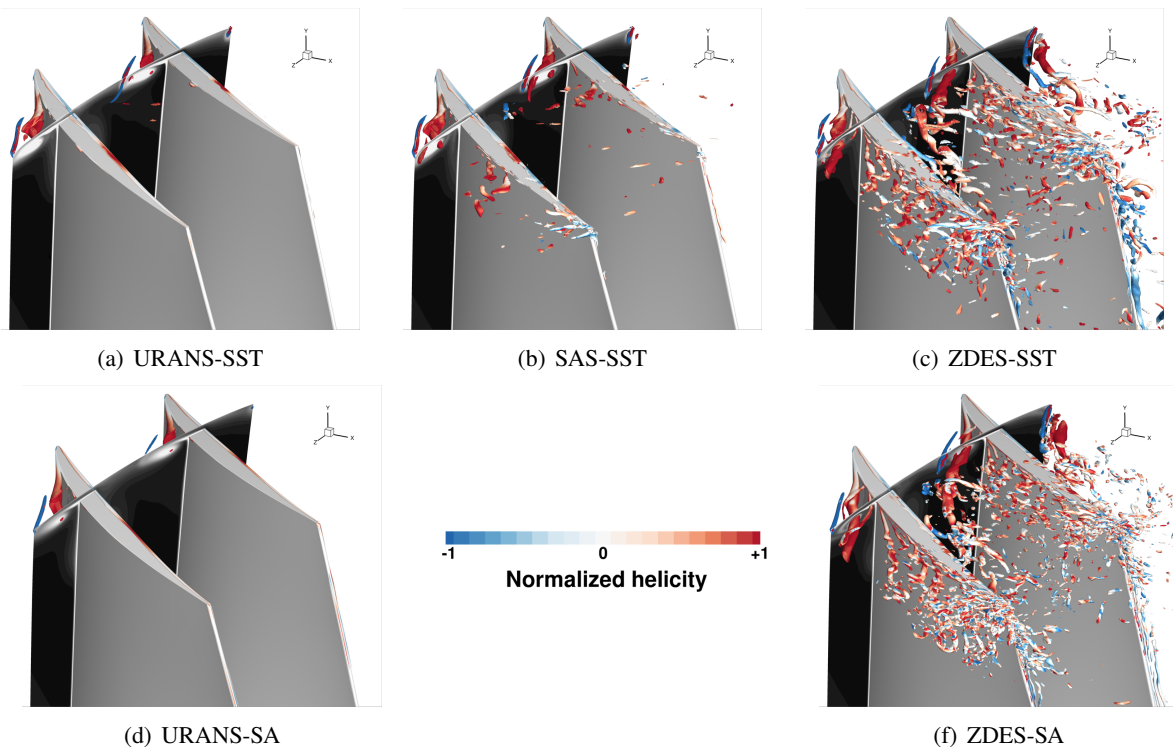


Figure 8: Snapshots of Q criterion iso-surface coloured by the normalized helicity and section 31% X/C filled with the entropy variation.

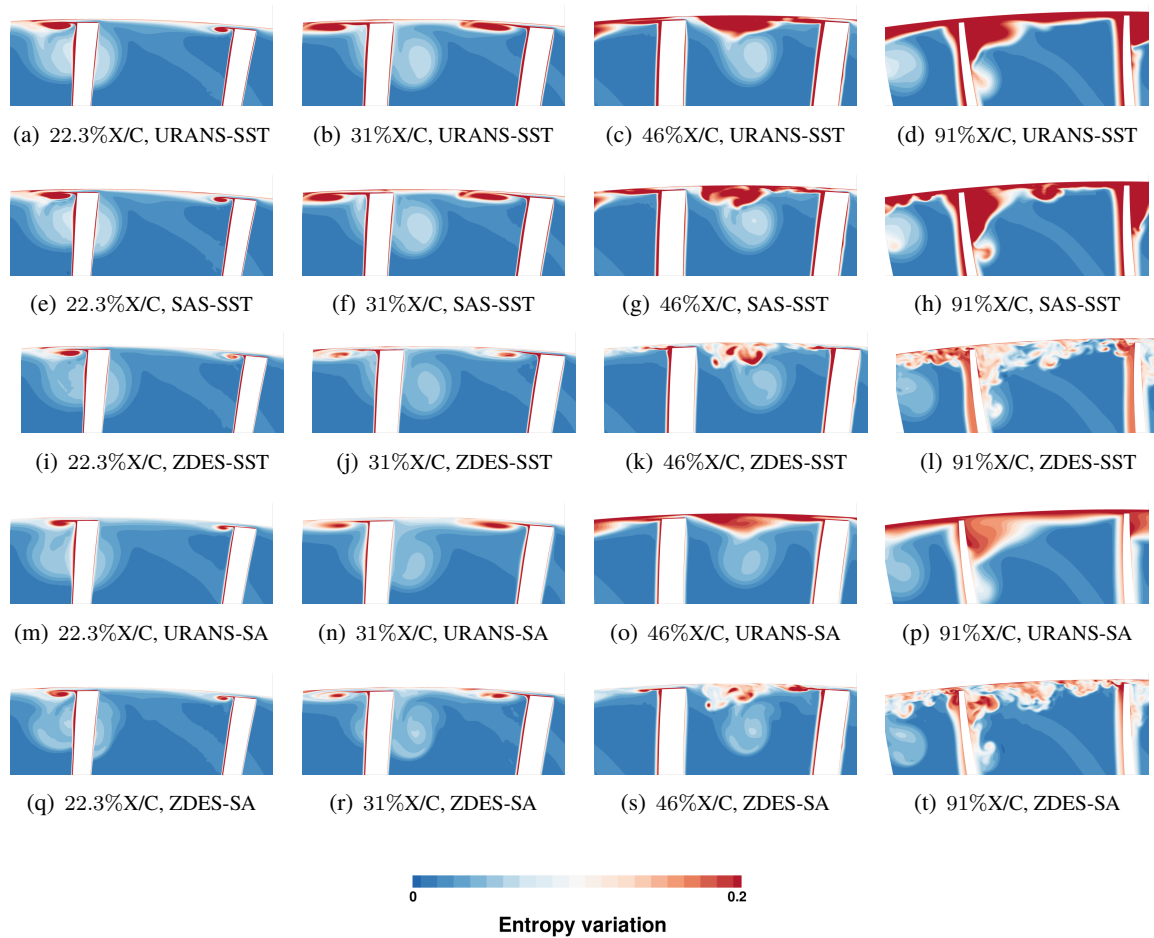


Figure 9: Entropy variation for four different axial positions at $t=nT$.

tion) for the five unsteady simulations (one line per simulation) for a given instant $t = nT$ i.e. after n IGV passing periods T . As the wall are considered as adiabatic, the entropy variation field is directly linked to the stagnation pressure loss. With entropy variation distribution, the boundary layers, wakes and vortices can be observed. It should be noticed that the coherent structures characterized by low to intermediary entropy variation level are relative to both IGV tip vortex and IGV wake. At the axial plane 22.3% X/C, the tip flow is quite similar for all simulations, even if the tip leakage vortex is slightly wider for SST turbulence model. At the chosen instant, the IGV tip vortex is observed in the vicinity of the left blade. Thus it allows to highlight the influence of this vortex on the development of the tip leakage vortex. This vortex is much more spread when it interacts with the IGV tip vortex and is very small otherwise. This interaction mechanism is responsible for the tip leakage vortex flutter phenomenon [Riéra et al., 2016]. From plane $x=31\%$ X/C. the flow predictions can be separated in two different categories. The first one is characterized by the strong dissipation of the tip leakage vortex leading to a wider high entropy area and thus to a significant stagnation pressure loss. The second category is characterized by a still small coherent tip leakage vortex and by numerous small secondary vortices. URANS-SA, URANS-SST and SAS-SST belong to the first category while the second category is composed of ZDES-SA and ZDES-SST computations. In the vicinity of blade trailing edge, the high-entropy areas of URANS-SST and SAS-SST are wider than URANS-SA and have a higher level. Thus the SST turbulence model is responsible for higher stagnation pressure loss as observed in absolute stagnation pressure radial distribution close to the casing (figure 6(a)). On the contrary, the entropy variation levels are smaller with ZDES-SST and ZDES-SA and the entropy field is composed of scattered high-entropy spots relative to the tip leakage vortex and to the multiple smaller secondary vortices. At plane 91% X/C, the small vortices are still observed. This plays a significant role in the stagnation pressure loss and explains why the stagnation pressure gradient is better predicted by ZDES methods in the vicinity of the casing.

The figure 10 shows the instantaneous entropy variation field at the experimental plane downstream of the first

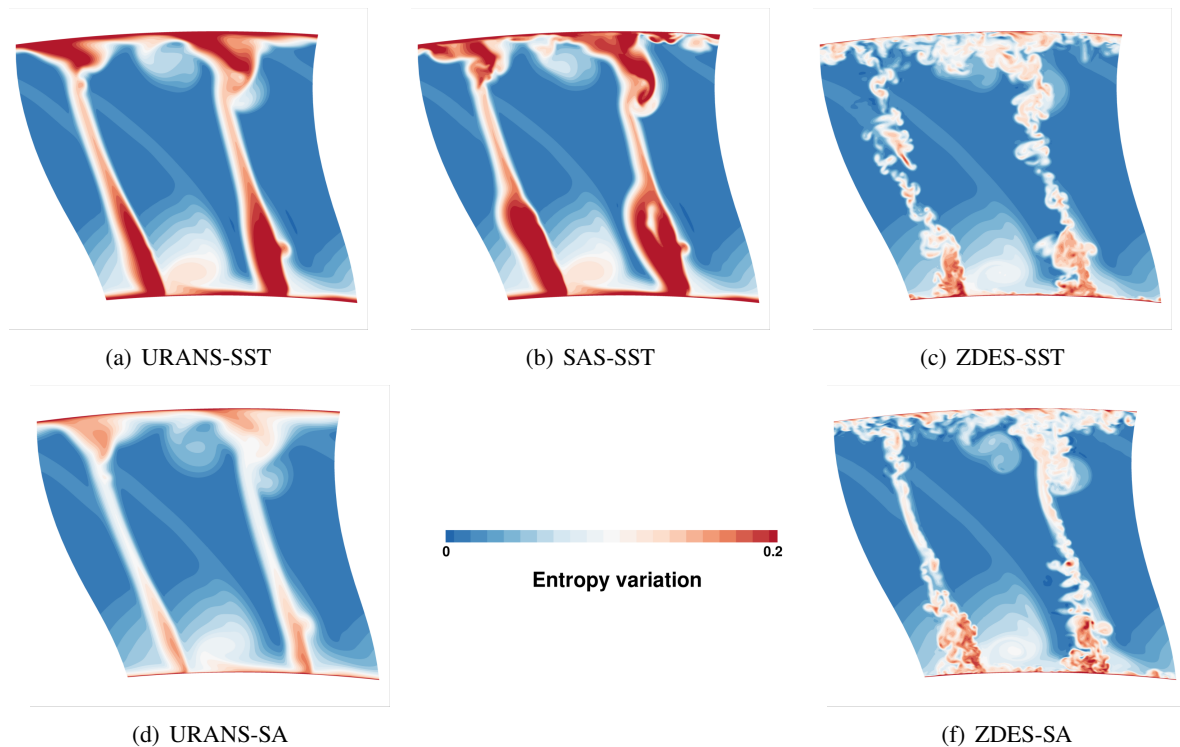


Figure 10: Entropy variation in plane 26A at $t=nT$.

rotor after n IGV passing periods. The IGV vortices and wake are still visible at the axial position. The highest stagnation pressure losses are predicted by URANS-SST and SAS-SST methods. Due to the reduction of turbulent viscosity (insufficient to have a LES behavior), the separation close to the hub is significantly amplified and the loss due to tip leakage flow is higher. It should be noticed that no significant separation are experimentally observed. Due to the tip leakage vortex dissipation and to a small separation on suction side close to the hub junction, URANS-SA predicts also losses but they are smaller than URANS-SST and SAS-SST. In all ZDES computations, the entropy is smaller and the areas of high entropy variation are thinner as they are relative to small coherent structures. Moreover, the losses due to hub and casing boundary layers are reduced using ZDES approach. The comparison between the two ZDES results shows that the losses are slightly higher close to the hub with SA turbulence model for the RANS part of the hybrid RANS/LES method, but this needs to be confirmed by the analysis of fully statistical converged results.

6 Conclusion

In the scope of this study, a ZDES reformulation above the $k - \omega$ Menter model with SST correction (referred as ZDES-SST) and the SAS method with αL correction (referred as SAS-SST) have been evaluated against previous ZDES-SA, URANS-SA, RANS-SA computations and concomitant URANS-SST, RANS-SST computations on a realistic rotor flow of a high-pressure compressor with incoming stator wakes at one nominal operating point. All simulations have been conducted in the same numerical framework, to the exception of RANS simulations which have been conducted on a coarser mesh for isospeed line exploration. The following conclusions can be drawn:

- URANS-SA and URANS-SST approaches led to the same results than their RANS counterparts, confirming the discrepancy between isospeed line depending of the turbulence model. URANS simulations are characterized by a low level of unsteadiness. Between all URANS and RANS simulations, URANS-SST and RANS-SST global performances predictions are closer to experimental values since these approaches result in higher losses than their SA counterparts.
- SAS-SST method with α to the default value of 2.5 has been unable to resolve a significant part of the largest

scale of turbulent motion, resulting in instantaneous field more similar to URANS results than ZDES ones. Tip leakage is slightly better predicted but the stagnation pressure losses are significantly increased.

- As ZDES-SA, ZDES-SST is able to capture the tip leakage vortex development and fluctuations of a wide range of scales, especially secondary vortices. However, the simulation duration is currently insufficient to clearly conclude about the improvement with respect to ZDES-SA. At least, the fluctuations involved in tip flow are only captured by ZDES approach, not by SAS method.

Ongoing ZDES-SST computation will be pursued for proceed to fully statically converged computation comparison.

As perspective, the evaluation of these methods will be performed in the context of rotor-stator interaction by included the following stator in the computational domain. Further interesting possibilities include to test the effect of the subgrid length scale based on the vorticity normal cell section Δ_ω instead of Δ_{vol} , to evaluate the potential improvement from high-order k -exact schemes [Maugars et al., 2014] and to conduct the presented simulations in near surge operating conditions.

7 Acknowledgments

The authors wish to thank gratefully W. Riéra who carried out the presented numerical test bench and URANS-SA/ZDES-SA simulations. The authors thank X. Ottavy (LMFA) for providing the experimental data, S. Deck and H. Bézard for their assistance on ZDES and SAS methods respectively as well as A. Le Pape, M. Costes and L. Castillon for their proofreading, data and useful discussions during this study. The authors are also grateful to B. Michel, B. Maugars, S. Heib and J. Mayeur, among others, for their help during ZDES-SST method implementation in ONERA's *elsA* solver. A part of the simulations presented in this article have been funded in the framework of the *elsA* three-party agreement between AIRBUS, SAFRAN, and ONERA which are co-owners of this software.

References

- G. Arroyo-Callejo, E. Laroche, P. Millan, F. Leglaye, and F. Chedevigne. Numerical Investigation of Compound Angle Effusion Cooling Using Differential Reynolds Stress Model and Zonal Detached Eddy Simulation Approaches. *Journal of Turbomachinery*, 2016.
- F. Benyoucef, H. Bézard, B. Aupoix, and B. Michel. SAS-SST model assessment and improvement. In *Conference on Modelling Fluid Flow (CMFF'12)*, 2012. URL <http://www.ara.bme.hu/ocs/index.php/cmff/cmff012/paper/view/80>.
- U. Bunge, C. Mockett, and F. Thiele. Guidelines for implementing Detached-Eddy Simulation using different models. *Aerospace Science and Technology*, 11(5):376–385, 2007.
- R.H. Bush and M. Mani. A two-equation large eddy stress model for high sub-grid shear. *AIAA paper*, 2561:2001, 2001. URL <http://arc.aiaa.org/doi/abs/10.2514/6.2001-2561>.
- L. Cambier, S. Heib, and S. Plot. The Onera *elsA* CFD software: input from research and feedback from industry. *Mechanics & Industry*, 14:159–174, 1 2013. ISSN 2257-7750. doi: 10.1051/meca/2013056.
- N. Chauvet, S. Deck, and L. Jacquin. Zonal Detached Eddy Simulation of a Controlled Propulsive Jet. *AIAA Journal*, 45(10): 2458–2473, 2007. doi: 10.2514/1.28562.
- H. Chuangxin, L. Yingzheng, and Y. Savas. A dynamic delayed detached-eddy simulation model for turbulent flows. *Computers & Fluids*, 146:174 – 189, 2017. ISSN 0045-7930. doi: <http://dx.doi.org/10.1016/j.compfluid.2017.01.018>. URL [/www.sciencedirect.com/science/article/pii/S0045793017300312](http://www.sciencedirect.com/science/article/pii/S0045793017300312).

- G. Comte-Bellot and S. Corrsin. Simple eulerian time correlation of full-and narrow-band velocity signals in grid-generated, 'isotropic' turbulence. *Journal of Fluid Mechanics*, 48(02):273–337, 1971. doi: 10.1017/S0022112071001599. URL <http://dx.doi.org/10.1017/S0022112071001599>.
- F. Daude. *Méthode d'intégration temporelle implicite pour la simulation des grandes échelles application à la réduction du bruit de cavité*. PhD thesis, Université de Poitiers, Poitiers, 2007.
- S. Deck. Recent Improvements in the Zonal Detached Eddy Simulation (ZDES) Formulation. *Theoretical and Computational Fluid Dynamics*, 26:523–550, 2012. ISSN 0935-4964. doi: 10.1007/s00162-011-0240-z. URL <http://dx.doi.org/10.1007/s00162-011-0240-z>.
- S. Deck and R. Laroüffé. Numerical investigation of the flow dynamics past a three-element aerofoil. *Journal of Fluid Mechanics*, 732:401–444, October 2013. ISSN 1469-7645. doi: 10.1017/jfm.2013.363.
- S. Deck, F. Gand, V. Brunet, and S. Ben Khelil. High-fidelity simulations of unsteady civil aircraft aerodynamics: stakes and perspectives. Application of zonal detached eddy simulation. *Philosophical Transactions of the Royal Society A: Mathematical, Physical and Engineering Sciences*, 372(2022):1–21, 2014. doi: 10.1098/rsta.2013.0325. URL <http://rsta.royalsocietypublishing.org/content/372/2022/20130325.abstract>.
- J.D. Denton. Loss Mechanisms in Turbomachines. *Journal of Turbomachinery*, 115:621–656, 1993. doi: 10.1115/1.2929299.
- J.R. Edwards and M-S. Liou. Low diffusion flux-splitting methods for flows at all speeds. In *AIAA*, volume 1862, pages 261–271, 1997.
- R. El Akoury, M. Braza, Y. Hoarau, J. Vos, G. Harran, and A. Sevrain. Unsteady flow around a NACA0021 airfoil beyond stall at 60° angle of attack. In *IUTAM Symposium on Unsteady Separated Flows and their Control*, pages 405–415, 2009.
- C.-C. Fan, X. Xiao, J.R. Edwards, H.A. Hassan, and R.A. Baurle. Hybrid Large-Eddy/Reynolds-Averaged Navier-Stokes Simulation of Shock-Separated Flows. *Journal of spacecraft and rockets*, 41(6):897–906, 2004. doi: <http://arc.aiaa.org/doi/abs/10.2514/1.3735>.
- M.S. Gritskevich, A.V. Garbaruk, J. Schütze, and F.R. Menter. Development of DDES and IDDES formulations for the $k - \omega$ Shear Stress Transport Model. *Flow, Turbulence and Combustion*, 88(3):431–449, 2012. ISSN 1386-6184. doi: 10.1007/s10494-011-9378-4. URL <http://dx.doi.org/10.1007/s10494-011-9378-4>.
- M.S. Gritskevich, A.V. Garbaruk, and F.R. Menter. Fine-tuning of DDES and IDDES formulations to the $k - \omega$ shear stress transport model. In *Progress in Flight Physics*, volume 5, pages 23–42. EDP Sciences, 2013. doi: <http://dx.doi.org/10.1051/eucass/201305023>.
- E. Guilmineau, G. Deng, and J. Wackers. Numerical simulation with a DES approach for automotive flows. *Journal of Fluids and Structures*, 27(5–6):807–816, 2011. ISSN 0889-9746. doi: <http://dx.doi.org/10.1016/j.jfluidstructs.2011.03.010>. URL <http://www.sciencedirect.com/science/article/pii/S0889974611000399>. IUTAM Symposium on Bluff Body Wakes and Vortex-Induced Vibrations (BBVIV-6).
- J.C. Kok. Resolving the dependence on freestream values for the $k - \omega$ turbulence model. *AIAA Journal*, 38(7):1292–1295, July 2000. URL <http://arc.aiaa.org/doi/abs/10.2514/2.1101>.
- J.C. Kok, H.S. Dol, B. Oskam, and H. van der Ven. Extra-large eddy simulation of massively separated flows. *AIAA*, 2004. doi: <http://arc.aiaa.org/doi/abs/10.2514/6.2004-264>. URL <http://arc.aiaa.org/doi/abs/10.2514/6.2004-264>.
- R. Laroüffé, S. Deck, and P. Sagaut. A dynamic forcing method for unsteady turbulent inflow conditions. *Journal of Computational Physics*, 230(23):8647–8663, 2011. ISSN 0021-9991. doi: <http://dx.doi.org/10.1016/j.jcp.2011.08.012>. URL <http://www.sciencedirect.com/science/article/pii/S0021999111004840>.
- D.K. Lilly. On the application of the eddy viscosity concept in the inertial sub-range of turbulence. Technical report, National Center for Atmospheric Research, 1966.
- J. Marty and B. Aupoix. Interaction of shrouded stator flow and main flow and its influence on performances of a three-stage high pressure compressor. *Proceedings of the Institution of Mechanical Engineers, Part A: Journal of Power and Energy*, 226(A4):489–500, 2012. ISSN 0957-6509. doi: 10.1177/0957650911414322.

- J. Marty, B. Aupoix, M. Schvallinger, and V.C. Sharma. Effet de la modélisation de la turbulence en proche pompage dans un compresseur multi-étages. In *AAAF, 43ème Colloque d'Aérodynamique Appliquée, Papier 14, Poitiers, France*, Mar. 10-12 2008.
- I. Mary, P. Sagaut, and M. Deville. An algorithm for low mach number unsteady flows. *Computers & Fluids*, 29:119–147, 2000. doi: 10.1016/S0045-7930(99)00007-9.
- B. Maugars, B. Michel, and P. Cinnella. High order and conservative method for patched grid interfaces. In *AIAA*, Atlanta, United States, June 2014. URL <https://hal-onera.archives-ouvertes.fr/hal-01069453>.
- F.R. Menter. Two-equation eddy-viscosity turbulence models for engineering applications. *AIAA Journal*, 32(8):1598–1605, August 1994. doi: <http://arc.aiaa.org/doi/abs/10.2514/3.12149>.
- F.R. Menter and Y. Egorov. A Scale Adaptive Simulation Model using Two-Equation Models. In *43rd AIAA aerospace sciences meeting and exhibit*, page 1095, 2005. URL <https://arc.aiaa.org/doi/abs/10.2514/6.2005-1095>.
- F.R. Menter and Y. Egorov. Revisiting the turbulent scale equation. In *IUTAM Symposium on One Hundred Years of Boundary Layer Research*, pages 279–290. Springer, 2006.
- F.R. Menter and Y. Egorov. The Scale-Adaptive Simulation Method for Unsteady Turbulent Flow Predictions. Part 1: Theory and Model Description. *Flow, Turbulence and Combustion*, 85(1):113–138, 2010. ISSN 1386-6184. doi: 10.1007/s10494-010-9264-5.
- F.R. Menter and M. Kuntz. Adaptation of eddy-viscosity turbulence models to unsteady separated flow behind vehicles. In *The Aerodynamics of Heavy Vehicles: Trucks, Buses, and Trains*, volume 19 of *Lecture Notes in Applied and Computational Mechanics*, pages 339–352. Springer Berlin Heidelberg, 2002. ISBN 978-3-642-53586-4. doi: <http://doi.org/b4xk>. URL <http://doi.org/b4xk>.
- M. Mersinligil, J-F. Brouckaert, N. Courtiade, and X. Ottavy. A High Temperature High Bandwidth Fast Response Total Pressure Probe for Measurements in a Multistage Axial Compressor. *Journal of Engineering for Gas Turbines and Power*, 134(061601):11, 2012. doi: 10.1115/1.4006061.
- U. Michel, D. Eschricht, B. Greschner, T. Knacke, C. Mockett, L. Panek, F. Thiele, and J. Yan. Simulation of the sound radiation of turbulent flows with DES. In *Proc. of the West-East High Speed Flow Field Conference*, pages 59–76, 2007.
- C. Mockett. *A Comprehensive Study of Detached Eddy Simulation*. PhD thesis, Fakultät V – Verkehrs- und Maschinensysteme der Technischen Universität Berlin, 2009.
- X. Ottavy, N. Courtiade, and N. Gourdain. Experimental and Computational Methods for Flow Investigation in High-Speed Multistage Compressor. *Journal of Propulsion and Power*, 28(6):1141–1155, 2012. doi: 10.2514/1.60562.
- K.R. Reddy, J.A. Ryon, and P.A. Durbin. A DDES model with a smagorinsky-type eddy viscosity formulation and log-layer mismatch correction. *International Journal of Heat and Fluid Flow*, 50:103 – 113, 2014. ISSN 0142-727X. doi: <http://dx.doi.org/10.1016/j.ijheatfluidflow.2014.06.002>. URL <http://www.sciencedirect.com/science/article/pii/S0142727X14000824>.
- A. Refloch, B. Courbet, A. Murrone, P. Villedieu, C. Laurent, P. Gilbank, J. Troyes, L. Tessé, G. Chaineray, J.B. Dargaud, E. Quémerais, and F. Vuillot. CEDRE Software. *AerospaceLab*, 2:p. 1–10, March 2011. URL <https://hal.archives-ouvertes.fr/hal-01182463>.
- N. Renard and S. Deck. Improvements in Zonal Detached Eddy Simulation for Wall Modeled Large Eddy Simulation. *AIAA Journal*, 53(11):3499–3504, 2015. doi: <http://arc.aiaa.org/doi/full/10.2514/1.J054143>.
- W. Riéra, J. Marty, L. Castillon, and S. Deck. Zonal Detached-Eddy Simulation Applied to the Tip-Clearance Flow in an Axial Compressor. *AIAA Journal*, 54(8):1–15, 2016. doi: <http://arc.aiaa.org/doi/abs/10.2514/1.J054438>.
- W. Riéra. *Evaluation of the ZDES method on an axial compressor: analysis of the effects of upstream wake and throttle on the tip-leakage flow*. Ph.D. thesis, Ecole Centrale de Lyon, November 2014. URL <https://tel.archives-ouvertes.fr/tel-01146424>.

- B. Sainte-Rose, N. Bertier, S. Deck, and F. Dupoirieux. Delayed Detached Eddy Simulation of a premixed methane-air flame behind a Backward-Facing Step. In *44th AIAA/ASME/SAE/ASEE Joint Propulsion Conference & Exhibit 21 - 23 July 2008, Hartford, CT*, volume 5134, page 2008, 2008. doi: <http://arc.aiaa.org/doi/abs/10.2514/6.2008-5134>.
- B. Sainte-Rose, N. Bertier, S. Deck, and F. Dupoirieux. A DES method applied to a backward facing step reactive flow. *Comptes Rendus Mécanique*, 337(6–7):340 – 351, 2009. ISSN 1631-0721. doi: <http://dx.doi.org/10.1016/j.crme.2009.06.017>. URL <http://www.sciencedirect.com/science/article/pii/S1631072109000813>. Combustion for aerospace propulsion.
- M.L. Shur, P.R. Spalart, M.K. Strelets, and A.K. Travin. Detached-eddy simulation of an airfoil at high angle of attack. In *Proceedings of the Fourth International Symposium on Engineering Turbulence Modelling and Measurements*, volume 4, pages 669–678, Ajaccio, Corsica, 24–26 May 1999. doi: 10.1016/B978-008043328-8/50064-3.
- J. Smagorinsky. General circulation experiments with the primitive equations: I. The basic experiment. *Monthly weather review*, 91(3):99–164, 1963.
- P.R. Spalart and S.R. Allmaras. A one-equation turbulence model for aerodynamic flows. In *30th Aerospace Sciences Meeting and Exhibit*, volume 94, Reno, NV, U.S.A., 1992. URL <http://arc.aiaa.org/doi/abs/10.2514/6.1992-439>.
- P.R. Spalart, W.H. Jou, M.K. Strelets, and S.R. Allmaras. Comments on the feasibility of LES for wings, and on a hybrid RANS/LES approach. In L Sakell C Liu, Z Liu, editor, *Advances in DNS/LES*, page 137–47, 1997.
- P.R. Spalart, S. Deck, M.L. Shur, K.D. Squires, M.K. Strelets, and A.K. Travin. A new version of detached-eddy simulation, resistant to ambiguous grid densities. *Theoretical And Computational Fluid Dynamics*, 20:181–195, 2006. doi: 10.1007/s00162-006-0015-0.
- H. Tartousi, P. Kulisa, F. Leboeuf, G. Ngo Boum, A. Lefebvre, and A. Yammine. Numerical Investigation of a Turbocharger Centrifugal Compressor: Volute Influence on the Performance of The Compressor. In M. Sen, G. Bois, M. Manna, and T. Arts, editors, *European Turbomachinery Conference, Istanbul, Turkey*, pages 1–10, March, 21–25 2011.
- A. Touyeras and M. Villain. Aerodynamic design and test result analysis of a three stage research compressor. In *ASME Turbo Expo: Power for Land, Sea, and Air, Vienna, Austria*, number GT2004-53940, pages 1–9, 2004.
- A.K. Travin, M.L. Shur, M.K. Strelets, and P.R. Spalart. Physical and Numerical Upgrades in the Detached-Eddy Simulation of Complex Turbulent Flows. In R. Friedrich and W. Rodi, editors, *Advances in LES of Complex Flows*, volume 65 of *Fluid Mechanics and Its Applications*, pages 239–254. Springer Netherlands, 2000. ISBN 978-1-4020-0486-5. doi: doi:10/bwdfxk.
- A.K. Travin, M.L. Shur, P.R. Spalart, and M.K. Strelets. Improvement of Delayed Detached-Eddy Simulation for LES with Wall Modelling. In *European Conference on Computational Fluid Dynamics, ECCOMAS CFD*. P. Wesseling, E. Oñate, J. Périaux, 2006.
- C. Uribe, J. Marty, and G. Gerolymos. Zonal Detached Eddy Simulation extension to $k - \omega$ models. In *Proceedings of the AIAA Aviation 2017, Denver, United States*, June 2017.
- D.C. Wilcox. Reassessment of the Scale-Determining Equation for Advanced Turbulence Models. *AIAA Journal*, 26(11): 1299–1310, November 1988. URL <http://arc.aiaa.org/doi/abs/10.2514/3.10041>.
- J. Yan, C. Mockett, and F. Thiele. Investigation of Alternative Length Scale Substitutions in Detached-Eddy Simulation. *Flow, Turbulence and Combustion*, 74(1):85–102, 2005. ISSN 1386-6184. doi: 10.1007/s10494-005-6916-y. URL <http://dx.doi.org/10.1007/s10494-005-6916-y>.
- J. Yan, L. Panek, and F. Thiele. Simulation of jet noise from a long-cowl nozzle with serrations. *AIAA Paper*, 3635:2007, 2007. URL <http://arc.aiaa.org/doi/abs/10.2514/6.2007-3635>.
- Z. Yin, K.R. Reddy, and P.A. Durbin. On the dynamic computation of the model constant in delayed detached eddy simulation. *Physics of Fluids (1994-present)*, 27(2):025105, 2015. doi: <http://dx.doi.org/10.1063/1.4907746>. URL <http://scitation.aip.org/content/aip/journal/pof2/27/2/10.1063/1.4907746>.

- X. Zheng, C. Liu, F. Liu, and C.-I. Yang. Turbulent transition simulation using the $k - \omega$ model. *International Journal for Numerical Methods in Engineering*, 42(5):907–926, 1998.
- L. Zhou, R. Zhao, and X.-P. Shi. An Entropy-Assisted Shielding Function in DDES Formulation for the SST Turbulence Model. *Entropy*, 19(3):93, 2017.